

“Sausage-string” appearance of arteries and arterioles can be caused by an instability of the blood vessel wall

JENS CHRISTIAN BRINGS JACOBSEN,¹ ULRİK BEIERHOLM,² RENE MIKKELSEN,²
FINN GUSTAFSSON,¹ PREBEN ALSTRØM,² AND NIELS-HENRIK HOLSTEIN-RATHLOU¹

¹*Department of Medical Physiology, The University of Copenhagen, DK-2200 Copenhagen N;*
and ²*The Niels Bohr Institute, The University of Copenhagen, DK-2100 Copenhagen Ø, Denmark*

Received 7 January 2002; accepted in final form 15 July 2002

Jacobsen, Jens Christian Brings, Ulrik Beierholm, Rene Mikkelsen, Finn Gustafsson, Preben Alstrøm, and Niels-Henrik Holstein-Rathlou. “Sausage-string” appearance of arteries and arterioles can be caused by an instability of the blood vessel wall. *Am J Physiol Regul Integr Comp Physiol* 283: R1118–R1130, 2002. First published July 25, 2002; 10.1152/ajpregu.00006.2002.—Vascular damage induced by acute hypertension is preceded by a peculiar pattern where blood vessels show alternating regions of constrictions and dilations (“sausages on a string”). The pattern occurs in the smaller blood vessels, and it plays a central role in causing the vascular damage. A related vascular pattern has been observed in larger vessels from several organs during angiography. In the larger vessels the occurrence of the pattern does not appear to be related to acute hypertension. A unifying feature between the phenomenon in large and small vessels seems to be an increase in vascular wall tension. Despite much research, the mechanisms underlying the sausage pattern have remained unknown. Here we present an anisotropic model of the vessel wall and show that the sausage pattern can arise because of an instability of the vessel wall. The model reproduces many of the key features observed experimentally. Most importantly, it suggests that the “sausaging” phenomenon is neither caused by a mechanical failure of the vessel wall due to a high blood pressure nor is it due to standing pressure waves caused by the beating of the heart. Rather, it is the expression of a general instability phenomenon. Experimental data suggest that the structural changes induced by the instability may cause secondary damage to the wall of small arteries and arterioles in the form of endothelial hyperpermeability followed by local fibrinoid necrosis of the vascular wall.

hypertension; vascular damage; rat; mathematical model

THAT BLOOD VESSELS have a regular cylindrical shape is an observation that at first sight does not appear to be in need of an explanation. However, there are several reports in the literature suggesting that the cylindrical shape may not be the preferred shape under all circumstances. Interestingly, it appears that vessels may also assume a stable pattern characterized by periodic constrictions and dilations. When severe experimental hypertension is induced by intravenous infusion of either

ANG II (15, 17), norepinephrine (30), or *N*^G-nitro-L-arginine methyl ester (L-NAME) (6), arterioles may develop a pattern of alternating constrictions and dilations along the vessel, giving rise to the so-called “sausage-string appearance” (Fig. 1) (6–8, 15, 17, 30). This vascular pattern has been demonstrated in small blood vessels in various vascular beds, including mesentery, intestine, kidney, eye, ear, and brain. The phenomenon is of a functional nature, since it disappears on lowering of the arterial pressure and reappears if the pressure is increased once more (16).

In the microcirculation the development of the sausage-string pattern is linked to the development of vascular damage. Endothelial hyperpermeability and exudation of macromolecules develop specifically in the dilated regions of the vessel (16, 17, 19, 20). This hyperpermeability is likely to be of clinical significance. It was noted already by Goldblatt (18) that arteriolar fibrinoid necrosis associated with severe hypertension is not distributed uniformly along the affected vessels. In fact, on microscopic examination of longitudinal sections of arterioles exposed to severe hypertension, areas dominated by fibrinoid necrosis alternate with apparently normal vascular wall segments (18). It is likely that this patchy distribution of arteriolar wall necrosis in malignant hypertension is a consequence of the peculiar sausage-string pattern that precedes the development of arteriolar lesions.

A remarkably similar vascular phenomenon has been observed in larger vessels during angiography (12, 23, 28). As in the microcirculation the vessels show periodic constrictions and dilations, and the phenomenon has been termed “stationary arterial waves” or “corrugated arteries” by different authors. It was first observed in femoral arteries (28, 29) but has subsequently been reported also in carotid, radial, splenic, superior mesenteric, and renal arteries (12). The striking pattern is stable, and it can appear on repeat angiograms obtained from a few minutes to a year later. Corrugations, however, disappear after administration of sympatholytic drugs, and it has not been possible to demonstrate any structural changes in the

Address for reprint requests and other correspondence: N.-H. Holstein-Rathlou, Dept. of Medical Physiology, The Panum Institute, 3 Blegdamsvej, DK-2200 Copenhagen N., Denmark (E-mail: nhhr@mfi.ku.dk).

The costs of publication of this article were defrayed in part by the payment of page charges. The article must therefore be hereby marked “advertisement” in accordance with 18 U.S.C. Section 1734 solely to indicate this fact.



Fig. 1. In vivo micrograph of rat intestinal arterioles showing a typical "sausage-string" pattern after induction of acute hypertension by intravenous infusion of ANG II. The accompanying vessels not showing constrictions and dilations are the corresponding venules. Scale bar in lower left corner, 100 μm . [Reproduced from Ref. 22 with permission.]

vessel wall that can explain the phenomenon. The phenomenon has been observed proximal from obstructive vascular lesions and in patients with various vascular diseases, e.g., thromboangiitis obliterans (Buerger's disease). In these large vessels, it has not been possible to establish any clinical consequences of corrugations (1, 12).

Several theories have been advanced to explain the occurrence of the regular pattern of constrictions and dilations (5, 12, 23). The dominant views have been that they are due either to some form of vascular spasm or that they are caused by a mechanical failure of the vessel wall (a blow out). However, these theories do not give a satisfactory explanation for the remarkable regularity and stability of the pattern.

In this paper we present a recently developed anisotropic, elastic model of the vessel wall (2) and show that under certain conditions an instability occurs that leads to a periodic pattern of constrictions and dilations along the vessel. The model provides predictions for the conditions under which the cylindrical form of the vessel becomes unstable, as well as for the physical characteristics of the pattern. We compare some of these theoretical predictions with simulated results as well as with experimental data obtained in rat intestinal arterioles during acute severe ANG II- or norepinephrine-induced hypertension.

METHODS

Experimental Studies

Animal preparation. Male Wistar rats (Panum Institute, Copenhagen, Denmark) ($n = 15$) weighing 187 ± 9 g or male Sprague-Dawley rats (Møllegaard, Lille Skensved, Denmark) ($n = 14$) weighing 199 ± 7 g were used for the experiments. The experimental protocol was approved by the National Research Animal Committee. Anesthesia was induced in a

chamber containing 5% halothane in a 35% O_2 -65% N_2 mixture followed by administration of 2% halothane in a 35% O_2 -65% N_2 mixture on a mask. Two polyethylene catheters (PE-10) were placed in the left jugular vein for infusions, and a catheter (PE-50) was inserted in the right carotid artery for continuous measurement of blood pressure (TBM4, World Precision Instruments, Aston, UK). Finally, a tracheostomy was performed to ensure unobstructed airways. After the initial surgical procedure, halothane anesthesia was replaced by intravenous infusion of pentobarbital sodium (120–150 $\mu\text{g}/\text{min}$). The animal was placed on a servocontrolled heated table maintaining body temperature at 37°C . After a median laparotomy, a loop (4–5 cm) of the jejunum was gently exteriorized and placed on a small stage slightly elevated from the table carrying the animal. A hole in the stage covered with a 40×24 mm covering glass allowed transillumination of the intestine. Using a microcautery, a 5-mm incision was made in the antimesenteric border of an empty intestinal segment. Subsequently, an approximately $1 \times 3 \times 30$ mm Sylgard (Dow Corning) block was introduced into the lumen of the intestine. The size of the Sylgard block was chosen to fill out the intestinal lumen, but care was taken not to stretch the intestinal wall and with it the vascular segments. The Sylgard block enabled sufficient transillumination for visualization purposes and protected against peristaltic movements of the intestinal segment under observation. The exteriorized intestine and mesentery were superfused with a 37°C physiological saline solution (0.9%) at a rate of 2–3 ml/min.

Observation of intestinal microcirculation and induction of hypertension. Microscopic observations of the intestinal microcirculation were begun after 30-min stabilization of the preparation. The intestinal microcirculation was observed using either a $4\times$ or a $10\times$ objective (Olympus, Tokyo) mounted on an upright microscope (BX50WI, Olympus). The field was viewed on a monitor (Trinitron, PWM 1442 QM, Sony, Tokyo) using a monochrome CCD camera (CCD 72S, DageMTI, Michigan City, IN), and recorded on videotape for off-line analysis. The final magnification of the image was approximately $\times 140$ with the $4\times$ objective and approximately $\times 350$ with the $10\times$ objective. The spatial resolution was ≈ 1 μm . The microscope was mounted on a motorized moveable stage (Micromanipulator Mini 25, Luigs and Neumann, Ratingen, Germany) that enabled easy observation of several points along the arterial tree under investigation. In the rat small intestine a small artery (subsequently referred to as A1) leaves the arcade artery along the mesenteric border and transverses approximately one-third of the intestine. In each experiment we studied one A1 and its branches (up to 4 lower branch orders, A2–A5) before and during the development of hypertension. The following parameters were recorded: branch order, resting diameter, appearance of sausage-string phenomena, minimal diameter during vasoconstriction, diameter, and length of localized dilations. In some experiments the time course of diameter changes was analyzed. In some experiments hypertension was relieved and reinduced to assess the reproducibility of the locations of localized dilations. Dilations occurring in relation to vessel bifurcations were not included in the analysis.

In the first series of experiments ($n = 15$, Wistar rats) hypertension was induced by continuous intravenous infusion of ANG II [50 $\mu\text{g}/\text{ml}$ at 20 $\mu\text{l}/\text{min}$ (1 $\mu\text{g}/\text{min}$) dissolved in 0.9% NaCl, Sigma Chemicals]. In the second series of experiments ($n = 12$, Sprague-Dawley rats) hypertension was induced by giving an initial fast infusion of ANG II (0.1–0.2 ml, 50 $\mu\text{g}/\text{ml}$ in 1–3 s) until a rise in blood pressure was observed. Thereafter ANG II was infused for another 10–20

s at 20 $\mu\text{l}/\text{min}$. After the ANG II infusion was interrupted, and when the blood pressure had returned to the control value (usually after 5–10 min), either ANG II ($n = 9$) or norepinephrine ($n = 3$) was given. The ANG II infusion in the second period was similar to the one given in the first period. Norepinephrine was given as an initial fast infusion (0.1–0.3 ml, 64 $\mu\text{g}/\text{ml}$ in 1–3 s) until a rise in blood pressure was observed. Thereafter a continuous infusion of norepinephrine (64 $\mu\text{g}/\text{ml}$ at 20 $\mu\text{l}/\text{min}$) was given for another 10–20 s. When the blood pressure returned to the control value, ANG II ($n = 12$) was given once more following the same protocol. In one experiment the last infusion period was continued for more than 20 min to test the long-term stability of the sausage pattern. In the final series of experiments ($n = 2$, Sprague-Dawley rats) hypertension was induced by giving an initial fast infusion of norepinephrine (0.1–0.3 ml, 64 $\mu\text{g}/\text{ml}$ in 1–3 s) until a rise in blood pressure was observed. Thereafter a continuous infusion of norepinephrine (64 $\mu\text{g}/\text{ml}$ at 20 $\mu\text{l}/\text{min}$ dissolved in 0.9% NaCl) was given for 10–20 s. After the norepinephrine infusion was interrupted, and when the blood pressure had returned to the control value (usually after 5–10 min), norepinephrine was given once more following the same protocol.

The Model

Kinetics of the vascular wall. The goal is to obtain a dynamic equation describing the local evolution of the internal radius r_i . Because blood is an incompressible fluid, a change in the internal radius of the vessel will be associated with a movement of the luminal fluid. Therefore, at a given point x along the length of the vessel, and at a given time t , the rate of change in the luminal cross-sectional area with time will be associated with a change in the volume flow J . From considerations of continuity it follows that

$$\partial_t(\pi r_i^2) = -\partial_x J \quad (1)$$

where $r_i = r_i(t, x)$ is the inner radius of the vessel. Ignoring inertial terms, the volume flow can be expressed as a function of the vascular conductance C and the local pressure gradient

$$J = -C(r_i)\partial_x P \quad (2)$$

It is assumed that the vascular conductance C can be described by the Hagen-Poiseuille relation

$$C(r_i) = \frac{\pi r_i^4}{8\eta} \quad (3)$$

where η is the viscosity.

Inserting Eq. 3 into Eq. 2 and differentiating with respect to x yields

$$\partial_x J = \partial_x \left(-\frac{\pi r_i^4}{8\eta} \partial_x P \right) \quad (4)$$

Inserting Eq. 4 into Eq. 1 yields an expression for the rate of change in internal radius at a given position along the vessel, that is

$$\partial_t r_i = \left(\frac{r_i^2}{4\eta} \right) \partial_x r_i \partial_x P + \left(\frac{r_i^3}{16\eta} \right) \partial_x^2 P \quad (5)$$

Mechanics of the vessel wall. The vessel wall is assumed to be in a near-equilibrium state. As a consequence, at each instance it can be assumed that the outward directed force due to the transmural pressure is balanced by the inward directed force by the vessel wall. It is further assumed that the rate of movement of the vessel wall is so slow that inertial

and viscous forces in the wall can be ignored. Finally the vessel wall is modeled as a layered structure where each layer carries a part of the transmural pressure P . The contribution of each layer is calculated by the differential form of Laplace's law (13, 14)

$$dP = \left(\frac{S}{R} + \frac{S_x}{R_x} \right) dr \quad (6)$$

where S and S_x are the circumferential and longitudinal stresses in a given layer of the vessel wall, respectively, and R and R_x are the radii of curvature of the layer in the circumferential and the longitudinal directions, respectively. The transmural pressure can then be calculated by integrating Eq. 6 through the vessel wall

$$P = \int_{r_i}^{r_i + \omega} \frac{S}{R} + \frac{S_x}{R_x} dr \quad (7)$$

where ω is the wall thickness. The two radii of curvature of a given layer are functions of their position within the vessel wall and can be expressed (9) as

$$\frac{1}{R} = \frac{1}{r[1 + (\partial_x r)^2]^{1/2}} \quad (8)$$

$$\frac{1}{R_x} = \frac{-\partial_x^2 r}{r[1 + (\partial_x r)^2]^{3/2}} \quad (9)$$

where r is the circumferential radius of the layer within the vessel wall.

The circumferential stress S is the force generated in the circumferential direction divided by the actual cross-sectional area of the vessel wall, F/A . It can be calculated from the idealized stress σ (force per relaxed cross-sectional area) (11), as

$$S = \sigma(1 + \epsilon) \quad (10)$$

where ϵ is the circumferential strain at a given position within the vessel wall. The circumferential strain is defined as $L/L_0 - 1$, where L is the actual length of the tissue, and L_0 is the length of the relaxed, unloaded tissue. Because the length of a vessel remains almost constant during a constriction, it is assumed that the stress in the longitudinal direction, S_x , is constant.

If ρ is the radial position of a layer within the relaxed vessel wall, and r is the radial position of the same layer in the constricted vessel wall, then it follows from the constant length of the vessel and the incompressibility of the vessel wall that the cross-sectional area between two layers remains constant, i.e., that

$$\rho^2 - \rho_i^2 = r^2 - r_i^2 \quad (11)$$

where ρ_i and r_i are the internal radius in the relaxed and constricted conditions, respectively. Rearranging and differentiating, we obtain

$$dr = \rho(\rho^2 - \rho_i^2 + r_i^2)^{-1/2} d\rho \quad (12)$$

Inserting Eqs. 8–12 into Eq. 7 and introducing the integration variable $z = \rho/\rho_i$ gives

$$P = \int_1^{\rho/\rho_i} \frac{z\rho_i^2\sigma(1 + \epsilon)}{(\rho^2 - \rho_i^2 + r_i^2)^{1/2}} \frac{1}{[1 + (\partial_x r)^2]^{1/2}} dz \quad (13)$$

$$+ S_x \int_1^{\rho/\rho_i} \frac{z\rho_i^2}{(\rho^2 - \rho_i^2 + r_i^2)^{1/2}} \frac{-\partial_x^2 r}{r[1 + (\partial_x r)^2]^{3/2}} dz$$

where ρ_o denotes the outermost layer. Note that $z = 1$ corresponds to the innermost layer of the wall and $z = \rho_o/\rho_i$ corresponds to the outermost layer. The circumferential strain ϵ in a given layer depends on its position within the wall and on the actual inner radius of the vessel (11)

$$\epsilon = \frac{1}{z} \sqrt{(r_i/\rho_i)^2 - 1 + z^2} - 1 \tag{14}$$

Simplifying Eq. 13 by inserting Eq. 14, we reach the final expression from which the transmural pressure can be obtained

$$P = \int_1^{\rho_o/\rho_i} \frac{\sigma}{z(\epsilon + 1)[1 + (\partial_x r)^2]^{1/2}} dz - S_x \int_1^{\rho_o/\rho_i} \frac{\rho_i \partial_x^2 r}{(\epsilon + 1)[1 + (\partial_x r)^2]^{3/2}} dz \tag{15}$$

The system is described by Eqs. 5 and 15. Equation 15 allows the calculation of the pressure profile along a vessel for a given longitudinal profile of the inner radius. The time derivative of the inner radius can then be calculated from Eq. 5, allowing the calculation of the longitudinal profile of the inner radius at the next time point.

Computations and Numerical Methods

The source code was written in C by the authors using Microsoft Developer Studio (Visual C++ 5.0 professional edition, Microsoft, Seattle, WA). Simulations were performed on a Sun Ultra80 workstation (Sun Systems, Palos Alto, CA), with a simulation of a single sausageing episode usually taking 10–20 days. The long computational time stems from the numerical (iterative) solution of the partial differential equations of the model. For the numerical integration of Eq. 5, a fourth-order Runge-Kutta scheme with stepwise adaptation of the size of the integration step was used (26).

Statistical Analysis

Data are presented as means \pm SE. Experimental data were compared using the Student's *t*-test. Regression lines were fitted by a standard least-squares method. A *P* value <0.05 was considered significant.

RESULTS

Experimental Studies

In the first series, infusion of ANG II at a rate of 1 $\mu\text{g}/\text{min}$ induced a typical sausage-string pattern in the small intestinal vessels in 9 of 15 rats. In the second series, using a faster initial infusion rate of ANG II, ANG II infusion induced the sausage-string pattern in 10 of 12 rats. In the third series, norepinephrine induced the sausage-string pattern in two of two rats. Although the protocols where the vasoactive substances are initially given as a fast infusion were slightly more successful in inducing the sausage pattern compared with the protocol using a constant infusion rate (86 vs. 60%), this difference was not statistically significant. Because the sausage-string patterns induced in the three series differed neither in shape nor in dimension, all the results in the three groups were pooled. There were no statistically significant

differences between the blood pressures in the rats that showed sausageing compared with the rats that did not show the pattern. In the first group the mean blood pressure increased from 103 ± 3 to 155 ± 4 mmHg ($n = 21$) during the infusion, and in the latter it increased from 97 ± 3 to 169 ± 6 mmHg ($n = 8$).

Figure 2 shows the distribution of the observed sausage-string patterns as a function of the preinfusion vascular diameter. When the sausage-string pattern occurred, it was present in a large number of vessels in the preparation. However, because of the experimental setup it was only possible to obtain optimal measurement conditions (e.g., good transillumination, clearly defined borders, no movements, several branch orders visible) for a few vessels in each rat. The sausage-string patterns were most frequently observed in the A2–A3 generation of arterial branches and were only rarely seen in the largest (A1) and the smallest (A4–A5) of the intestinal vessels. Figure 3 shows the time course for the development of sausage-string patterns in two vessels from two rats in the second and third series. The time courses were the same regardless of whether ANG II or norepinephrine was infused. After start of the rapid infusion, the pattern occurs after 10 s, and it is fully developed within 5–10 s (Fig. 3A). Notice that the maximal radius of the “sausage” actually exceeds the preinfusion radius. If the infusion of ANG II (1 $\mu\text{g}/\text{min}$) was maintained, the sausage-string pattern could be observed for >20 min (Fig. 3B). In the first series where ANG II was infused a constant rate throughout, the sausage pattern developed gradually over 5–10 min (not shown). The length of the individual sausages increased linearly as a function of the preinfusion vessel diameter (Fig. 4). The line in Fig. 4 is the best fit through the origin.

The pattern was both reversible and reproducible. As illustrated in Fig. 5, the sausage pattern disappeared

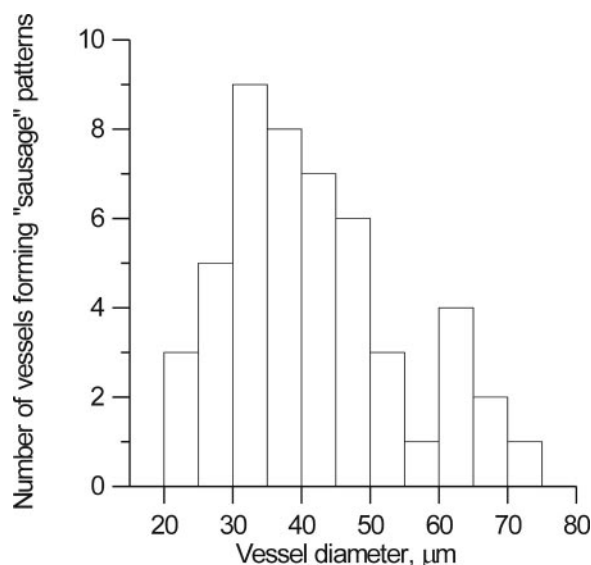


Fig. 2. Distribution of the observed sausage-string patterns as a function of the preinfusion vessel diameter. A total of 49 vessels were observed to form a sausage pattern in 21 rats.

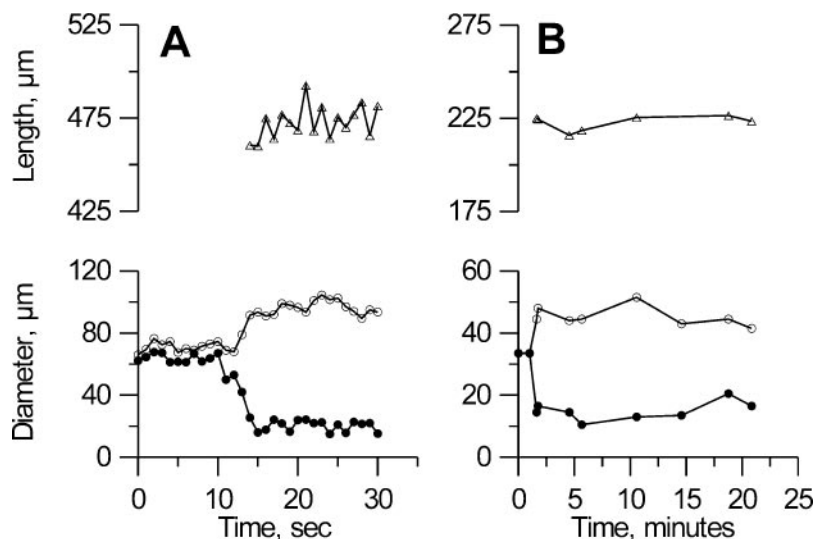


Fig. 3. Time course of “sausage” length (Δ), and maximal (\circ) and minimal (\bullet) diameters in 2 vessels as the sausage patterns developed. *A*: short-term response to infusion of norepinephrine (NE). *B*: long-term response to a prolonged infusion of ANG II. The intravenous infusions were begun at time 0 s.

~5 min after the ANG II infusion was interrupted, and it reappeared after consecutive infusions of either ANG II (Fig. 5A) or norepinephrine (Fig. 5B). When the ANG II or norepinephrine infusion was repeated in the 12 rats from series 2 and 3 that had shown the sausage-string pattern during the initial infusion period, sausage-string patterns reappeared in a total of 7 rats. The dilations and constrictions developed at the same sites along the vessel during the repeated infusion periods (Fig. 5), and the pattern of constrictions and dilations were the same when norepinephrine and ANG II were infused consecutively to the same rat (Fig. 5B).

Simulation Studies

Figure 6A shows a theoretical stress-strain curve for a piece of vascular tissue during maximal activation of the smooth muscle cells. Note that the curve includes both the active stress due to the contraction of the vascular smooth muscle cells and the passive stress due to the collagen and the elastic fibers of the vessel wall. During vasoconstriction the strain in the differ-

ent layers depends on their position within the vessel wall (cf. Eq. 14). The two filled circles in Fig. 6A indicate the respective strain-stress values in the innermost and the outermost layers of the wall of a constricted vessel with an inner resting radius (ρ_i) of 15 μm , an actual inner radius (r_i) of 4 μm , and a wall-to-lumen ratio $[(\rho_o - \rho_i) / \rho_i]$ of 0.1. As shown previously (2), if the point corresponding to the outermost layer lies below the line through the origin and the point corresponding to the innermost layer (the dotted line in Fig. 6A), the cylindrical shape of the vessel is unstable. Thus, after a small perturbation, it will not return to the cylindrical shape. Figure 6B illustrates the same vessel at the same transmural pressure, but now only at ~50% activation of the vascular smooth muscle cells. In this case, the point corresponding to the outermost layer is above the dotted line, and the cylindrical shape of the vessel is stable (2).

Figure 7 shows the result of a simulation using parameters corresponding to Fig. 6A. The cylindrical shape was perturbed by adding a random number between -5×10^{-2} and $5 \times 10^{-2} \mu\text{m}$ to the inner radius (see Fig. 7, box). At $t = 1 \times 10^{-5}$ s, some of the variation in the inner radius has disappeared, and as time progresses the perturbation grows in amplitude, while the wavelength of the perturbation increases. After ~0.02 s the pattern is stable, and the vessel now shows a typical sausage pattern with alternating constrictions and dilations.

To fulfill the instability criterion outlined in Fig. 6, it is necessary that the stress-strain curve is relatively flat over a range of strains, i.e., that there is a part of the curve where the stress is relatively independent of the strain. This is illustrated in Fig. 8, where we used different shapes of the stress-strain curve for the computations. As the relatively flat portion of the stress-strain curve is reduced, the region where the instability occurs is also smaller. However, it is clear that the occurrence of a sausage-string pattern is not critically dependent on the specific shape of the stress-strain curve. From Fig. 8B it can also be seen that increasing

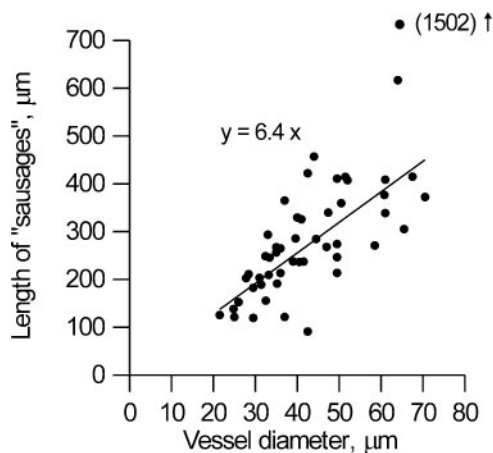


Fig. 4. Length of sausages as a function of the preinfusion diameter of the vessel. The straight line represents the best fit through the origin ($y = 6.4x$). Coefficient of determination (R^2) is 0.91; $P < 0.01$.

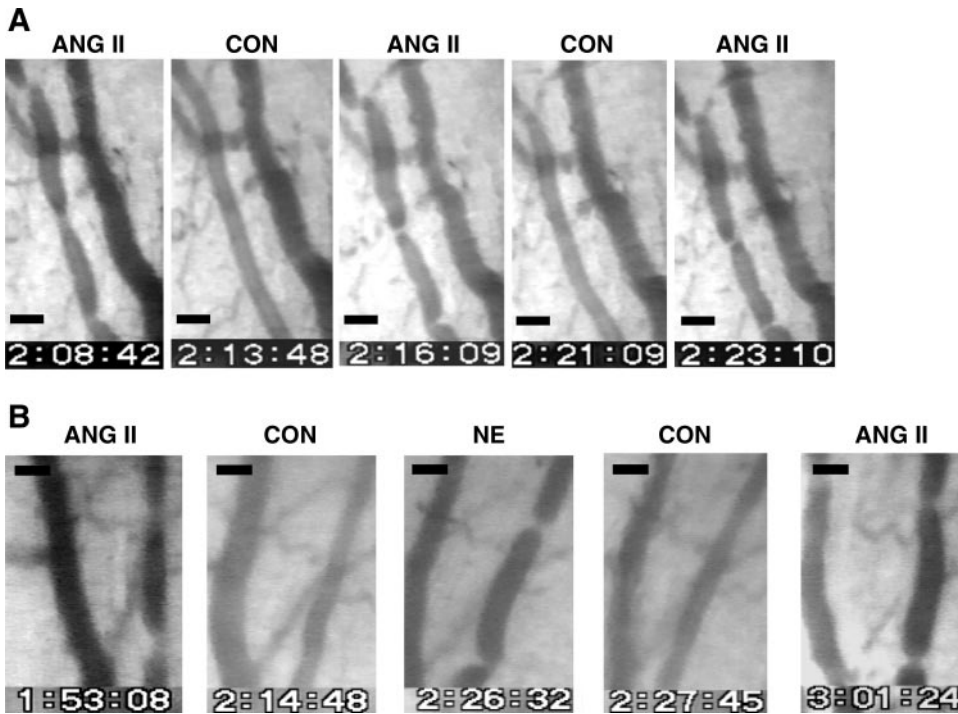


Fig. 5. Effect of repeat infusions of ANG II and/or NE. *A*: when the ANG II infusion was interrupted (CON), the sausage-string pattern disappeared, and it reappeared at the same sites on repeat infusions of ANG II. Scale bar at bottom left corner, 50 μm . *B*: as with the infusion of ANG II, infusion of NE also caused the appearance of the sausage-string pattern. Notice that the pattern seen during NE infusion is identical to that seen during ANG II infusion. Scale bar at top left corner, 50 μm . CON, infusion of saline.

the wall-to-lumen ratio decreases the region where the instability will occur. A thick-walled vessel will therefore be less prone to develop the instability.

The shape of the stress-strain curve influences the shape of the “sausages.” Figure 9 shows the result of a simulation where the flat portion of the stress-strain curve is reduced in length (coarse dashed line in Fig. 8A). When the flat portion is reduced in length, the constrictions become somewhat less pronounced. Also shown in Fig. 9 is the pressure in the vessel during the development of the sausage pattern. Initially the pressure tends to be higher in the constricted regions compared with the dilated regions (cf. Fig. 9, top). This is not due to differences in the degree of activation of the vascular smooth muscle because this is assumed to be similar and maximal in all parts of the vessel. Rather, it is a consequence of the law of Laplace. Due to the flat part of the stress-strain curve the tension in the wall is

relatively stable as the vessel either constricts or dilates. Because the pressure is approximately inversely proportional to the circumferential radius (cf. Eq. 6) the pressure will increase in regions that constrict and decrease in regions that dilate. The pressure difference inside the vessel will then cause further shifts in the intravascular blood volume so that blood will move from the constricted to the dilated regions, thereby reinforcing the development of the sausage pattern. Ultimately, as can be seen in the bottom panel, the system reaches a new mechanical equilibrium where the blood has redistributed and the intravascular pressure again is the same throughout the vessel.

The sausage-string pattern occurred over a wide range of parameter values. However, the geometrical characteristics of the “sausages” varied as the different parameter values were changed. Figure 10 shows how the sausages become elongated as the wall-to-lumen

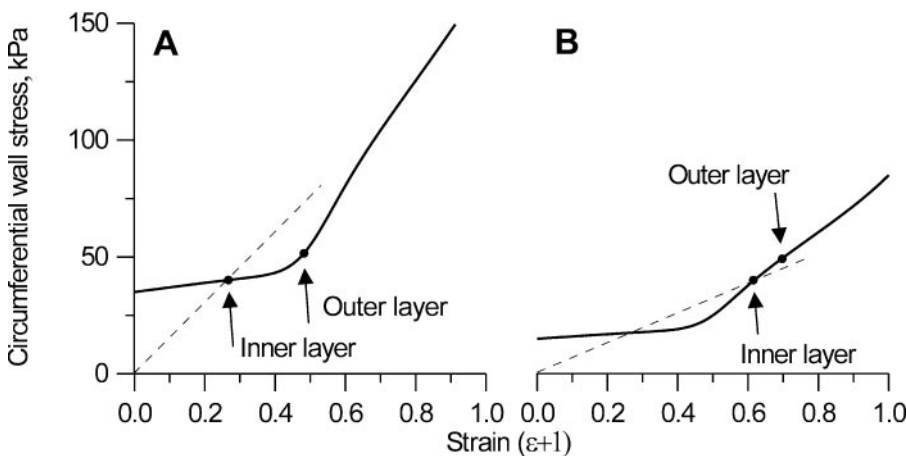


Fig. 6. Schematic plot of stress (σ)-strain (ϵ) relations for an arteriole. *A*: solid line corresponds to the stress-strain relation for an arteriole with maximal activation of the vascular smooth muscle cells. The dots on the solid line indicate the corresponding values of stress and strain in the innermost and outermost layers of the vessel at a given internal diameter. If the dot corresponding to the outermost layer is below the line through the origin and the dot corresponding to the innermost layer (dotted line), the cylindrical shape will be unstable. *B*: here the solid line corresponds to the stress-strain relation of an arteriole at half-maximal activation. In this case the dot corresponding to the outermost layer is above the line through the origin and the dot corresponding to the innermost layer. Consequently the cylindrical shape of the vessel is stable. See text for details.

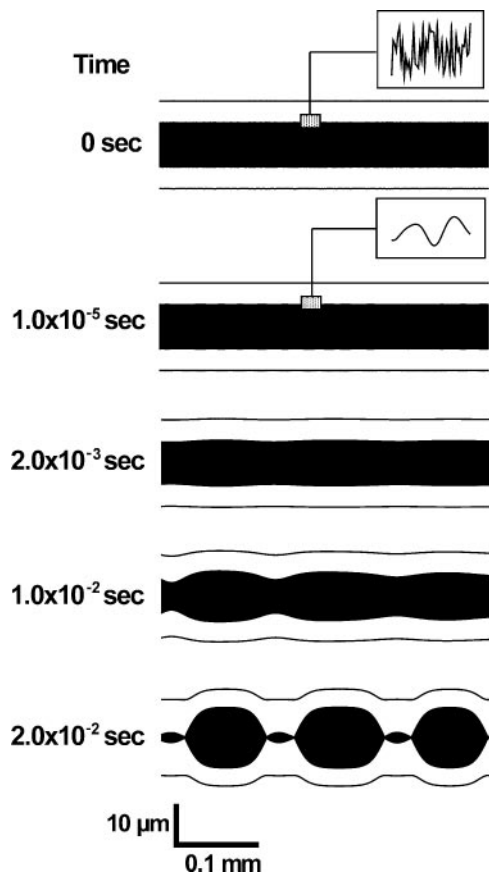


Fig. 7. Evolution of the sausage pattern. At *time 0* the cylindrical shape is perturbed by adding random numbers between -5×10^{-2} and $5 \times 10^{-2} \mu\text{m}$ to the inner radius. The box represents a blow up ($1.5 \times$ on *x*-axis and $100 \times$ on *y*-axis) of the inner diameter of the vessel. After 10^{-5} s the shape of the vessel has already been smoothed by the disappearance of the highest frequencies of the initial perturbation (see box) that represents a blow up of the innermost diameter. As time progresses there is a gradual increase in the amplitude and the wavelength of the perturbation. After $\sim 2 \times 10^{-2}$ s, a stable sausage pattern has developed. Notice that the figure is not drawn to scale. For this simulation, initial $r_i = 4 \mu\text{m}$ and $\rho_i = 15 \mu\text{m}$, where r_i and ρ_i are the internal radii in the constricted and relaxed conditions, respectively; resting wall-to-lumen ratio $[(\rho_o - \rho_i)/\rho_i] = 0.1$; and longitudinal stress (S_x) = 10 kPa.

ratio $[(\rho_o - \rho_i)/\rho_i]$ is increased. At the lowest wall-to-lumen ratio, the pattern is more like pearls on a string. For larger, more realistic values of the wall-to-lumen ratio, both the dilated and the constricted regions elongate, and the shape becomes closer to that seen experimentally (Fig. 10B)

A critical parameter is the longitudinal stress S_x . There is little information in the current literature as to its magnitude. We therefore performed simulations where the magnitude of this parameter was varied by a factor of 10. As can be seen from Fig. 11, as the longitudinal stress increased, the length between the constrictions increased. From the linear theory outlined in the APPENDIX, we expect that the length of the sausages increases with the square root of the longitudinal stress. This is confirmed by the results of the simulations. In Fig. 11 we have fitted a square root relation between the length of the sausages and the

longitudinal stress. There is good agreement between the results of the simulations and the theoretical predictions. The slight scatter of the simulation results around the regression line is due, at least in part, to the use of a random initial perturbation. This will cause a slight variation in the final shape of the pattern despite all other parameters being equal. Interestingly, the computational burden increased considerably as the longitudinal stress increased. At the lowest values of the stress, the simulations would be finished within a couple of days, whereas for the largest values of the stress investigated, the simulations required close to 3 wk to complete.

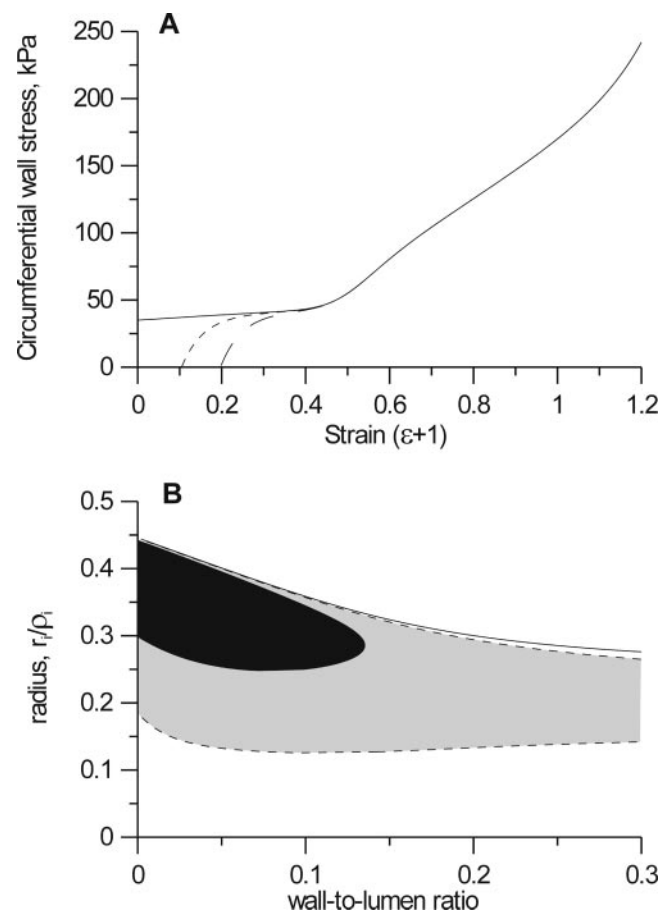


Fig. 8. A: 3 different stress-strain relations for an arteriole at maximal activation. The stress-strain relation represented by the solid curve is the same as the relation shown in Fig. 6A. The stress-strain relation represented by the fine dashed line (short dashes) has a shortened flat portion at the lowest values of the strain, and this is even more pronounced for the stress-strain relation represented by the coarse dashed line (long dashes). B: regions where the cylindrical shape becomes unstable. For the stress-strain curve represented in A by the solid line, the cylindrical shape of the vessel will be unstable when the normalized inner radius (r_i/ρ_i) is reduced below the solid line. The value of r_i/ρ_i where the instability occurs decreases with increasing wall-to-lumen ratios. The light gray area indicates the region of r_i/ρ_i and wall-to-lumen ratios where the cylindrical shape of the vessel is unstable for the stress-strain curve represented by the fine dashed line in A. The black area represents the corresponding area of instability for the stress-strain curve represented by the coarse dashed line in A. As the flat portion of the stress-strain curve is reduced, the area of the region where the instability occurs is reduced. In all simulations, S_x was 10 kPa.

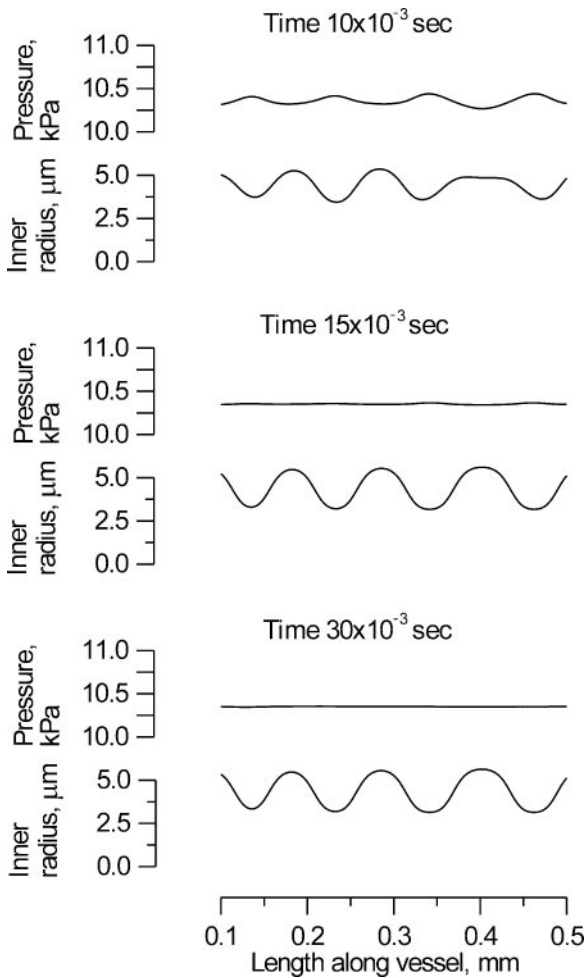


Fig. 9. Time course of the inner radius and the transmural pressure during the development of the sausage pattern. For this simulation the stress-strain curve given by the coarse dashed line in Fig. 8A was used. The time refers to time after the perturbation. After 10^{-1} s the transmural pressure is uniform along the vessel, indicating that the vessel has attained a new steady state. For this simulation initial $r_i = 4.5 \mu\text{m}$, $\rho_i = 15 \mu\text{m}$, resting wall-to-lumen ratio = 0.1, and $S_x = 10 \text{ kPa}$.

There is a direct linear relationship between the length of the sausages and the resting radius of the vessel (Fig. 12). As the resting radius increases, the length of the sausages also increases. Thus small vessels will tend to form short sausages, whereas larger vessels will have longer sausages during the instability. Again there is a good agreement between the simulations and the predictions from the linear theory (cf. APPENDIX). The same linear relationship between vessel size and sausage length was also present in the experimental data (cf. Fig. 4). Notice, however, that the slopes were significantly different, with the slope estimated from the experimental data being 3.5 times that found in the simulations.

DISCUSSION

Although it has been known for decades that arteries and arterioles can assume a shape characterized by regular, symmetric, and alternating areas of constric-

tions and dilations, the mechanism(s) underlying this phenomenon has remained an enigma (1, 12, 22). The results of the present study suggest that under certain conditions the normal, cylindrical shape of a blood vessel may become unstable, and as a result the vessel exhibits a periodic pattern of constrictions and dilations.

The peculiar pattern of constrictions and dilations has been described both in the microcirculation using in vivo microscopy and in larger vessels during arteriography (15, 16, 22, 24, 28). Despite the remarkable similarity in the characteristics of the phenomenon in large and small vessels, the investigations on the un-

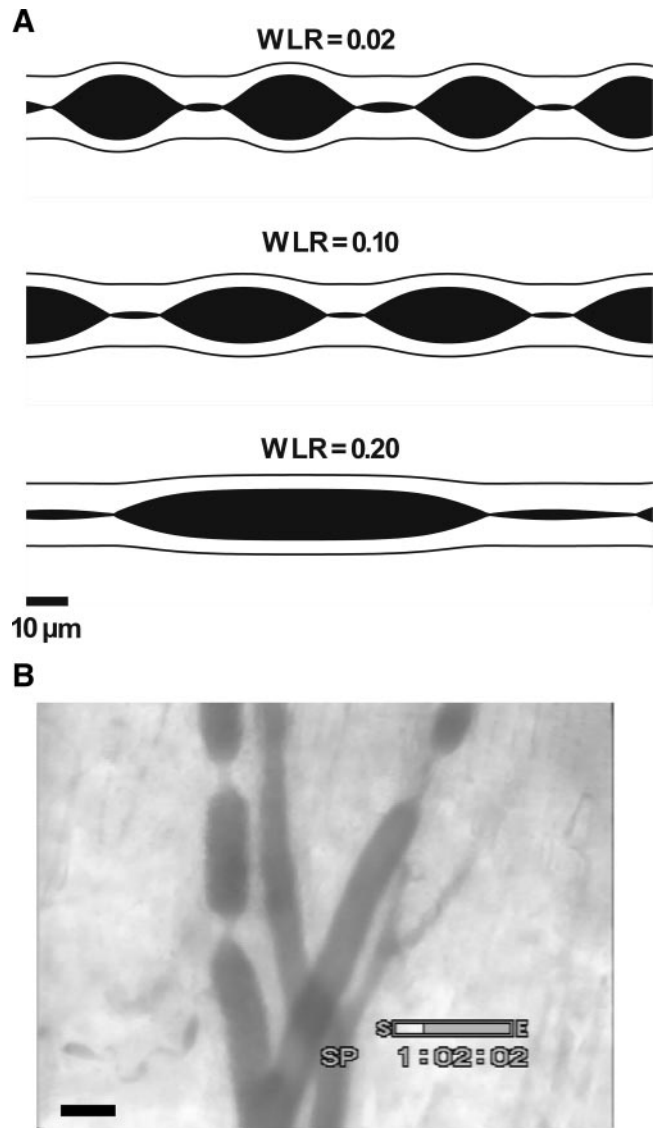


Fig. 10. A: sausage pattern at 3 different wall-to-lumen ratios [$\text{WLR} = (\rho_o - \rho_i) / \rho_i$]. For a very thin-walled vessel ($\text{WLR} = 0.02$), the individual sausages are fairly short. For a slightly thicker wall ($\text{WLR} = 0.1$), the sausages are elongated. This is even more pronounced as the WLR is increased to 0.2. For these simulations, initial $r_i = 4 \mu\text{m}$, $\rho_i = 15 \mu\text{m}$, and $S_x = 10 \text{ kPa}$. B: high-magnification view of sausages on an intestinal arteriole. Notice that both the sausages and the constrictions are elongated, resembling the simulations above with $\text{WLR} = 0.2$. Scale bar in bottom left corner, $50 \mu\text{m}$.

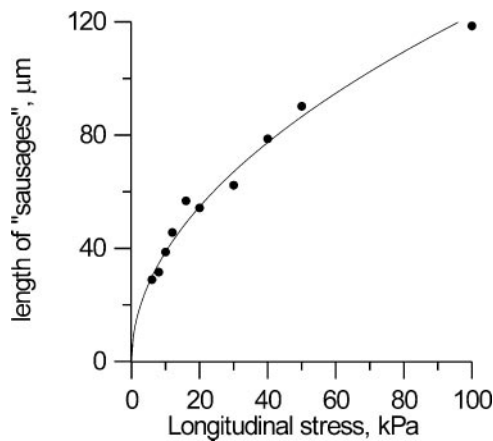


Fig. 11. Sausage length as a function of S_x . The solid line represents the best fit of the relation $y = ax^{1/2}$, where $a = 12.2 \mu\text{m} \cdot \text{kPa}^{-1/2}$ ($R^2 = 0.98$, $P < 0.01$). The scatter of the simulated data is due to the use of a random initial perturbation. For these simulations, initial $r_i = 4 \mu\text{m}$, $\rho_i = 15 \mu\text{m}$, and resting wall-to-lumen ratio = 0.1.

derlying mechanism(s) appear to have progressed independently within their respective fields. Characteristically the pattern appears to be functional. There are, at least initially, no morphological distinctions between the constricted and the dilated areas (15, 22). The pattern is highly reproducible. In the microcirculation the phenomenon is typically seen during periods with high blood pressure, induced for example by intravenous infusion of ANG II. If the hypertension is abolished, the uniform arteriolar structure is restored. Elevating the pressure once more causes the reappearance of the sausage pattern. Likewise, in larger vessels the corrugations can be abolished by infusion of sympatholytic substances, and it will reappear on termination of the infusion (12). Another spectacular feature of the phenomenon is its periodicity with constrictions and dilations occurring in a highly regular and repetitive pattern.

Several explanations have been advanced to explain the occurrence of the periodic pattern of constrictions and dilations (5, 12, 22, 23, 24). In the microcirculation, the dominating view has been that the phenomenon represented a blow out of the vessel wall. Thus, due to high blood pressure, the vessel wall suffers a fatigue and the local dilations appear. This hypothesis, however, is unable to explain the periodic nature of the phenomenon. Also, it is problematic that sausaging occurs in the peripheral part of the vascular tree (cf. Figs. 1 and 2) where the pressure increase will be modest due to the pressure drop along the upstream vessels. In larger vessels it has been suggested that the corrugations seen on angiograms could be an artefact due to an interface disturbance between the contrast medium and the blood (23). This fails however to explain the stationary characteristics of the phenomenon over longer time periods, as well as other features (12). It has also been suggested that the corrugations could be due to standing arterial pressure waves (24). However, the arterial pulse wave has a wavelength much

larger than the observed distances between the constrictions (12–14).

The unifying feature connecting the sausage pattern in microvessels and the corrugations in large vessels seems to be an increase in circumferential wall stress (1, 22). In the microvessels this is typically caused by the infusion of vasoactive substances like ANG II, norepinephrine, or L-NAME, which activates the vascular smooth muscle cells causing increased wall tension, arteriolar constriction, and increased blood pressure (6, 15, 17, 30). In the larger vessels it is suggested that the increased circumferential wall stress is due to activation of the vascular smooth muscle cells secondary to local diseases in the vessel wall (e.g., thromboangiitis obliterans and peripheral obstructive lesions) (12, 28).

It could be argued that the periodic pattern reflects a spatial heterogeneity in the distribution of receptors on the vascular smooth muscle cells or a heterogeneity in the distribution of the contractile filaments along the vessel. These possibilities cannot be excluded from the present observations. However, the main conclusion from the present work is that such a heterogeneity is not a necessity for explaining the appearance of periodic constrictions and dilations. A uniform increase in the tone of the vascular smooth muscle cells along a homogeneous vessel can, under some circumstances, lead to the formation of a periodic pattern of constrictions and dilations. In support of this interpretation is the fact that the sausage-string pattern does not depend on the specific nature of the infused vasoactive agent. Rather, as also demonstrated in the present study, it can be induced by a variety of vasoactive substances (6, 15, 17, 30).

It may seem counterintuitive that a uniform increase in wall tension results in the loss of the cylindrical shape, and the formation of a pattern characterized by periodic constrictions and dilations. The instability is related to the well-known instability responsible for the breakup of a cylinder of fluid into droplets (the

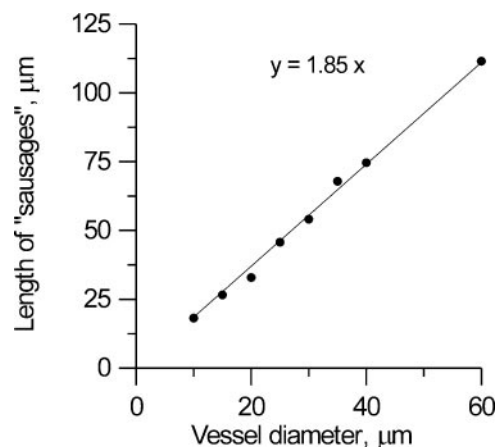


Fig. 12. Sausage length as a function of resting vessel diameter ($2\rho_i$). The solid line is the best linear fit through the origin ($R^2 = 0.999$, $P < 0.01$). For these simulations, initial $r_i = 4\rho_i/15$ (thus the degree of constriction was the same irrespective of vessel size), and $S_x = 10 \text{ kPa}$.

Rayleigh instability) (25, 27). In a fluid the constrictions will lead to a physical separation of the column, and thereby the formation of droplets. A vessel will of course maintain its coherent structure. Recently a similar instability has been described in tubular lipid membranes (3, 4). When the membrane tension was increased by local illumination with a laser beam, a similar pattern of constrictions and dilations occurred. This has been termed the “pearling” instability.

The critical feature necessary for the instability to occur is that the stress-strain curve has a relatively flat portion, i.e., that there is a region where the stress is relatively stable even though the strain changes (Fig. 6). We hypothesize that such a region could exist at low radii at maximal or near-maximal activation of the vascular smooth muscle cells. As the vessel constricts due to the infusion of, for example, ANG II, it will enter this region of the stress-strain curve. Consequently, the cylindrical shape will become unstable, and the sausage pattern will emerge.

The instability does not depend critically on the shape of the stress-strain curve. This is illustrated in Fig. 8 where simulations were done for different shapes of the stress-strain curve. As the flat portion of the stress-strain curve was shortened, the range of radii where the instability occurs is decreased. For the curve with the largest flat portion, the instability occurs when the radius r_i is reduced below 30–40% of the resting value ρ_i . In contrast, when the flat portion was shortened from the left, the cylindrical shape regains its stability when the radius is reduced to values below the flat portion of the curve (Fig. 8). It should be emphasized that it is not a requirement for the instability to occur that the stress-strain curve has one of the shapes used in the present simulations (cf. Figs. 6 and 8). The only condition that needs to be fulfilled is that illustrated in Fig. 6. Thus there should be a region where the operating point for the outer layer of the vessel wall falls below the line through the origin and the operating point corresponding to the inner layer (2). Clearly, there are many possible stress-strain curves that fulfill this quite general criterion. On the other hand, despite similar increases in blood pressure, not all rats and not all vessels of a similar size in the same rat showed the sausage pattern. One explanation for this observation could be that the stress-strain curves in these cases did not fulfill the instability criterion. This would not be surprising, considering that stress-strain curves obtained from different vessels show considerable variation (10).

In the present study we used two infusion protocols. The only difference in the results between the two was the time course of the sausage pattern. Not surprisingly, when the vasoactive compound was infused at a rapid initial rate, the pattern developed faster compared with when a constant, relatively slow infusion rate was used. The sausage pattern emerged ~ 10 s after the initiation of the fast infusion of either ANG II or norepinephrine, and it was fully developed within 5–10 s (cf. Fig. 3). This is slower than the time course found in the simulations where the pattern was fully

developed within 0.02 s of the initial perturbation. There is, however, no major discrepancy here, because the 10–15 s *in vivo* includes the time necessary for the vasoactive substance to reach the local site and to increase the vascular tone to the level where the instability occurs. The speed by which the pattern develops in the simulated data merely indicates that when the vessel has passed the point of instability (the critical point), the new equilibrium state is attained fast. In contrast, in the experiments the vessel is initially in a stable condition. As the vasoactive substance is infused and the plasma levels increase, the stress-strain relation gradually changes due to the increasing activation of the vascular smooth muscle cells. After some time the vessel will reach the critical point, and it will assume the sausage pattern. As the vessel moves past the critical point (due to the continued infusion of the vasoactive agent), the amplitude of the “sausages” will increase smoothly and the pattern will become more pronounced.

The resulting shape of the sausages will depend on the characteristics of the vessel. The model predicts that the length of the individual sausages depends on the size of the vessel. In a large vessel the constrictions will be further apart compared with a vessel with a smaller diameter (cf. Fig. 12). This is in agreement with the experimental findings. As is evident from Fig. 4, there appears to be a linear relationship between the preinfusion diameter of the vessel and the length of the individual sausages. A similar linear relationship between vessel diameter and wavelength of the corrugations has been reported for large arteries (12, 24). Although there was a linear relationship between vessel size and sausage length in both the experimental and the simulated data, the slope of the linear relationship was larger in the experimental data compared with the simulated data. One reason for this discrepancy is that the experimentally determined diameters are not resting values, but rather represent the normal, partly constricted state of the vessel. Therefore, the resting diameters will exceed the preinfusion diameters used in Fig. 4, and consequently, the slope would have been smaller had we used resting diameters instead. Also, the length of the sausages depends on the values of the parameters used in the simulation. Using a larger wall-to-lumen ratio increases the length of the sausages and will therefore give a larger slope for the regression line. A second important parameter that influences the length of the dilated regions and thereby the slope of the regression line is the longitudinal stress S_x . There is little information in the literature as to the size of the longitudinal stress in the vessel wall. However, it is probably safe to assume that it will be at least of the same order of magnitude as the transmural pressure (13, 14). Within this region, the length of the sausages increases with the longitudinal stress. Therefore, using a larger value of the longitudinal stress would also increase the slope of the regression line between vessel diameter and sausage length. Because the computational time increases considerably with increasing values for S_x , we deliberately used

a low value for this parameter in the simulations. The linear analysis suggests that the length should scale with the square root of the longitudinal stress, and this is confirmed by the simulations. It is also possible that a more elaborate model would give a better fit. In particular, the present model assumes that the longitudinal stress is constant both as the shape of the wall changes and in the different layers of the vessel wall. This is clearly a simplification that could influence the predicted size of the sausage length.

As the wall-to-lumen ratio is increased, the dilated areas become more elongated. This may explain why the corrugations seen in large vessels are more like pearls on a string than the corresponding structures seen in the microcirculation, where the pattern resembles sausages on a string. It is well known that the wall-to-lumen ratio increases as arterial vessels get smaller (13, 14). Large vessels will therefore show dilated regions that are shorter relative to the radius of the vessel compared with small vessels (Fig. 10). Consequently, the pattern will resemble pearls on a string rather than sausages on a string in the larger vessels. Figure 8 shows that vessels with larger wall-to-lumen ratios in general will be more stable compared with vessels with thinner walls. As mentioned above, the wall-to-lumen ratio increases as the arterial vessels get smaller. This may explain why the sausage pattern is rarely observed in the smallest arterioles (Fig. 2).

The functional significance of the periodic pattern of constrictions and dilations remains unresolved. There do not appear to be any clinical correlates to the occurrence of corrugations observed in larger arteries on angiograms. However, the sausage pattern seen during severe hypertension in small arteries and arterioles appears to be associated with significant functional alterations in the vascular wall. It has been a consistent finding that a hyperpermeability develops in the dilated regions (16, 19, 20). This hyperpermeability is associated with the deposition of macromolecules in the vascular wall of the dilated regions (5, 15, 16). Whether this local deposition of macromolecules is associated with or results in the patchy lesions of fibrinoid necrosis that is seen during severe cases of hypertension (malignant hypertension) remains unresolved.

An interesting consequence of the present theory is that the increased permeability observed in the dilated regions does not represent a simple pressure effect. Indeed, only vessels where the pressure increase is modest will destabilize (cf. Fig. 6), and the instability is not associated with local increases in the transmural pressure (cf. Fig. 9). Rather, the increased permeability may represent an active endothelial response to the changes in the flow patterns and/or the shear stresses elicited by the shape change. This is supported by recent experimental studies that have shown that the increased permeability, but not the "sausaging" phenomenon itself, can be blocked by inhibitors of endothelin, a vasoactive peptide produced by the endothelial cells (6).

A limitation of the present theory is the neglect of the branching structure of the circulation. Dilations seem to be especially prevalent at branching sites (7, 8, 15, 16), a fact not accounted for by the simple theory presented here. A branching site has unique elastic properties, and the flow and pressure patterns differ significantly from those found in the cylindrical portions of the vessel. Furthermore, the present model does not incorporate a longitudinal flow along the vessel. We do not expect that this presents a major problem. In the microcirculation, the sausaging is associated with a nearly complete termination of the longitudinal flow as the constrictions are narrow enough to restrict the movement of red blood cells. We therefore expect that the assumption of a nearly uniform transmural pressure will be an acceptable approximation to the situation in vivo.

The present model does not include wall viscosity. Adding wall viscosity will slow the speed by which the sausage pattern develops, but it will not prevent the occurrence of the instability. Including wall viscosity in the model is equivalent to increasing blood viscosity. As can be seen from the stability analysis outlined in the APPENDIX, the viscosity term does not enter into the critical equation (Eq. A6). The instability is solely dependent on shape of the stress-strain relation.

During pronounced vasoconstriction, the luminal surface of the vessel may fold and form longitudinal ridges (21). In the present model it is assumed that the individual layers remain circular even during maximal vasoconstriction. However, it is unlikely that this simplification is a problem. The main mechanical effect of the folding is that below a given level of constriction, the layer loses the ability to generate tangential force (21). This feature is already included in the model. As can be seen from Fig. 8, even in situations where the layers lose the ability to provide tangential force below a certain level of constriction, it is still possible for the instability to occur.

There was good agreement between the results of the linear analysis (given in the APPENDIX) and the results of the computer simulations (Figs. 11 and 12). In a complex model like the present it is inherently difficult to evaluate the adequacy of the numerical methods used in the simulations. However, the simulations and the linear analysis are two independent solutions of the model equations, and the good agreement between the two provides strong support for the adequacy and the correctness of the numerical methods used in the simulations.

In summary, in the present mathematical model of a homogeneous vessel, a uniform increase in wall tension induces a pattern characterized by periodic constrictions and dilations. Such patterns have been observed both in large and small blood vessels. The model reproduces many of the key features observed experimentally. Most importantly, it suggests that the sausaging phenomenon is neither caused by a mechanical failure of the vessel wall due to a high blood pressure, nor is it due to standing pressure waves caused by the beating of the heart. Rather, it is the expression of a general

instability phenomenon. Experimental data suggest that the structural changes induced by the instability may cause secondary damage to the vessel wall of small arteries and arterioles in the form of endothelial hyperpermeability followed by local fibrinoid necrosis.

APPENDIX

Several analytical expressions can be derived from the model Eq. 15

$$P = \int_1^{\rho_o/\rho_i} \frac{\sigma}{z(\epsilon + 1)[1 + (\partial_x r)^2]^{1/2}} dz - S_x \int_1^{\rho_o/\rho_i} \frac{\rho_i \partial_x^2 r}{(\epsilon + 1)[1 + (\partial_x r)^2]^{3/2}} dz \tag{A1}$$

This can be simplified significantly by considering only small perturbations of the vessel wall (2)

$$P = \int_1^{\rho_o/\rho_i} \frac{\sigma - \sigma_x r \partial_x^2 r}{(z^2 - 1 + r_i/\rho_i^2)^{1/2}} dz \tag{A2}$$

where σ_x is the idealized stress in the longitudinal direction.

This can be further reduced by considering a perturbation of the radius $r \rightarrow r + u(z)$, and only retaining terms up to the first order

$$P = P_0(r) + I(r)u - I_0(r)\partial_x^2 u \tag{A3}$$

with

$$P_0(r) = \int_1^{\rho_o/\rho_i} \frac{\sigma}{(z^2 - 1 + r_i/\rho_i^2)^{1/2}} dz \tag{A4}$$

$$I_0(r) = \sigma_x r_i \int_1^{\rho_o/\rho_i} \frac{1}{(z^2 - 1 + r_i/\rho_i^2)^{1/2}} dz = \sigma_x r_i \log \left[1 + \frac{\rho_o - \rho_i + r_o - r_i}{\rho_i + r_i} \right] \tag{A5}$$

and

$$I(r) = \frac{d}{dr} P_0(r) = \rho_i \int_1^{\rho_o/\rho_i} z^{-1} \frac{d}{dr} \left(\frac{\sigma}{\epsilon + 1} \right) dz \tag{A6}$$

The simplified expression for the pressure P (Eq. A3) can now be inserted into Eq. 5. If we ignore the mixed term $\partial_x r_i \partial_x P$, it can be shown that a small periodic perturbation $u = u_k(t) \cos(kz)$ will develop as $u_k(t) \sim u_k(0)e^{\lambda_k t}$, where the time constant λ_k is given by

$$\lambda_k = \frac{C(r)}{2\pi r} k^2 [-I(r) - I_0(r)k^2] \tag{A7}$$

The perturbation will grow for λ_k positive. $I_0(r)$ is always positive (cf. Eq. A5). Thus it is the sign of $I(r)$ (Eq. A6) that determines the stability of the vessel wall. If $I(r)$ is positive, the cylindrical shape is stable (λ_k is negative and the perturbation decreases in size). If $I(r)$ is negative, there will be a value of k ($= 2\pi/\text{wavelength}$) below which λ_k will be positive, and where the perturbation will therefore increase in size.

The dominant (fastest growing) wave number k , as found by setting the derivative of λ_k equal to zero, will then be given by

$$k = (|I|/2I_0)^{1/2} \tag{A8}$$

The wavelength of the “sausages,” l , is the inverse of k times 2π

$$l = 2\pi \sqrt{\frac{2I_0}{|I|}} \sim \sqrt{\sigma_x} \tag{A9}$$

Thus the length of the sausages varies as the square root of the idealized stress in the longitudinal direction. Insertion of typical values for the parameters of the model yields

$$l \approx 2\pi \rho_i \tag{A10}$$

Hence, the length of the sausages will increase linearly with the resting radius of the vessel, and the length will be approximately 5 to 10 times the radius of the relaxed vessel.

We thank Dr. T. Griffith, Univ. of Cardiff (Cardiff, UK) for drawing our attention to the literature on corrugated arteries.

This work was supported by grant from the Novo-Nordisk Foundation, the Danish Medical Research Council, and the Danish Heart Association.

REFERENCES

1. Adams DF and Lebowitz RL. Corrugated arteries. Fixed pathology or functional alterations? *Arch Surg* 104: 18–19, 1972.
2. Alström P, Equiluz VM, Colding-Jørgensen M, Gustafsson F, and Holstein-Rathlou N-H. Instability and “sausage-string” appearance in blood vessels during high blood pressure. *Phys Rev Lett* 82: 1995–1998, 1999.
3. Bar-Ziv R and Moses E. Instability and “pearling” states produced in tubular membranes by competition of curvature and tension. *Phys Rev Lett* 73: 1392–1395, 1994.
4. Bar-Ziv R, Tlusty T, Moses E, Safran SA, and Bershadsky A. Pearling in cells: a clue to understanding cell shape. *Proc Natl Acad Sci USA* 96: 10240–10145, 1999.
5. Beilin LJ and Goldby FS. High arterial pressure versus humoral factors in the pathogenesis of the vascular lesions of malignant hypertension. The case for pressure alone. *Clin Sci Mol Med* 52: 111–117, 1977.
6. Bouriquet N, Dupont M, Herizi A, Mimran A, and Casellas D. Preglomerular sudanophilia in L-NAME hypertensive rats. Involvement of endothelin. *Hypertension* 27: 382–391, 1996.
7. Byrom FB. The pathogenesis of hypertensive encephalopathy and its relation to the malignant phase of hypertension. Experimental evidence from the rat. *Lancet* 2: 201–211, 1954.
8. Byrom FB. The evolution of acute hypertensive arterial disease. *Prog Cardiovasc Dis* 17: 31–37, 1974.
9. Do Carmo MF. *Differential Geometry of Curves and Surfaces*. Englewood Cliffs, NJ: Prentice-Hall, 1976.
10. Davis MJ and Gore RW. Length-tension relationship of vascular smooth muscle in single arterioles. *Am J Physiol Heart Circ Physiol* 256: H630–H640, 1989.
11. Feldberg R, Colding-Jørgensen M, and Holstein-Rathlou N-H. Analysis of the interaction between TGF and the myogenic response in renal blood flow autoregulation. *Am J Physiol Renal Fluid Electrolyte Physiol* 269: F581–F593, 1995.
12. Foster JH, Killen DA, and Klatt E. Corrugated arteries—an enigma. *Am Surg* 34: 398–412, 1968.
13. Fung YC. *Biomechanics. Mechanical Properties of Living Tissues* (2nd ed). New York: Springer-Verlag, 1990.
14. Fung YC. *Biomechanics. Motion, Flow, Stress, and Growth*. New York: Springer-Verlag, 1990.
15. Giese J. *The Pathogenesis of Hypertensive Vascular Disease*. Copenhagen, Denmark: Munksgaard, 1966.
16. Giese J. Acute hypertensive vascular disease. 2. Studies on vascular reaction patterns and permeability changes in by means of vital microscopy and colloidal tracer technique. *Acta Pathol Microbiol Scand* 62: 497–515, 1964.
17. Giese J. Renin, angiotensin, and hypertensive vascular disease. *Am J Med* 55: 315–332, 1973.

18. **Goldblatt HJ.** Studies on experimental hypertension. VII. The production of the malignant phase of hypertension. *Exp Med* 67: 809–826, 1938.
19. **Goldby FS and Beilin LJ.** Relationship between arterial pressure and the permeability of arterioles to carbon particles in acute hypertension in the rat. *Cardiovasc Res* 6: 384–390, 1972.
20. **Goldby FS and Beilin LJ.** How an acute rise in arterial pressure damages arterioles. *Cardiovasc Res* 6: 569–584, 1972.
21. **Greensmith JE and Duling BR.** Morphology of the constricted arteriolar wall: physiological implications. *Am J Physiol Heart Circ Physiol* 247: H687–H698, 1984.
22. **Gustafsson F.** Hypertensive arteriolar necrosis revisited. *Blood Press* 6: 71–77, 1997.
23. **Mayall GF.** A model for the study of stationary arterial waves. *Clin Radiol* 17: 84–85, 1966.
24. **New PFJ.** Arterial stationary waves. *Am J Roentgenol Radium Ther* 97: 488–499, 1966.
25. **Plateau J.** *Statique Experimentale et Theorique des Liquides Soumis aux Seules Forces Moleculaires.* Paris: Gautier-Villars, 1873.
26. **Press WH, Teukolsky SA, Vetterling WT, and Flannery BP.** *Numerical Recipes in C: The Art of Scientific Computing* (2nd ed). Cambridge, UK: Cambridge Univ. Press, 1993.
27. **Rayleigh L.** On the instability of a cylinder of viscous liquid under capillary force. *Philos Mag* 34: 145–154, 1892.
28. **Theander G.** Arteriographic demonstration of stationary arterial waves. *Acta Radiol* 53: 417–425, 1960.
29. **Weickbom I and Bartley O.** Arterial “spasm” in peripheral arteriography using the catheter method. *Acta Radiol* 47: 433–448, 1957.
30. **Wilson SK, Steinsland OS, and Nelson S.** Isolated, perfused rabbit ear artery: a model for studying segmental vasoconstriction and dilatation. *J Cardiovasc Pharmacol* 23: 127–135, 1994.

